Research Article

Cumulant-Based Coherent Signal Subspace Method for Bearing and Range Estimation

Zineb Saidi[1] and Salah Bourennane[2]

[1] EA 3634, Institut de Recherche de École Navale (IRENav), École Navale, Lanvéoc Poulmic, BP 600, 29240 Brest-Armées, France
[2] Institut Fresnel, UMR CNRS 6133, Université Paul Cézanne Aix-Marseille III, EGIM, DU de Saint Jérôme, 13397 Marseille Cedex 20, France

A new method for simultaneous range and bearing estimation for buried objects in the presence of an unknown Gaussian noise is proposed. This method uses the MUSIC algorithm with noise subspace estimated by using the slice fourth-order cumulant matrix of the received data. The higher-order statistics aim at the removal of the additive unknown Gaussian noise. The bilinear focusing operator is used to decorrelate the received signals and to estimate the coherent signal subspace. A new source steering vector is proposed including the acoustic scattering model at each sensor. Range and bearing of the objects at each sensor are expressed as a function of those at the first sensor. This leads to the improvement of object localization anywhere, in the near-field or in the far-field zone of the sensor array. Finally, the performances of the proposed method are validated on data recorded during experiments in a water tank.

1. INTRODUCTION

Noninvasive range and bearing estimation of buried objects, in the underwater acoustic environment, has received considerable attention.

Many studies have been recently developed. Some of them use acoustic scattering to localize objects by analyzing acoustic resonance in the time-frequency domain, but these processes are usually limited to simple shaped objects [1]. In the same way, Guillermin et al. [2] use the inversion of measured scattered acoustical waves to image buried object, but the applicability in a real environment is not proven. Another method which uses a low-frequency synthetic aperture sonar (SAS) has been recently applied on partially and shallowly buried cylinders in a sandy seabed [3]. Other techniques based on signal processing, such as time-reversal method [4], have been also developed for object detection and localization but their applicability in real life has been proven only on cylinders oriented in certain ways and point scatterers [5]. Furthermore, having techniques that operate well for simultaneous range and bearing estimation using wideband and fully correlated signals scattered from near-field and far-field objects, in a noisy environment, remains a challenging problem.

Array processing techniques, such as the MUSIC method, have been widely used for source localization. Typically, these techniques assume that the underwater acoustic sources are on the seabed and are in the far field of the sensor array. The goal then is to determine the directions of the arrival of the sources. These techniques have not been used yet for bearing and range estimation for buried objects.

In this paper, the proposed approach is based on array processing methods combined with an acoustic scattering model. The fourth-order cumulant matrix [6, 7] is used instead of the cross-spectral matrix to remove the additive Gaussian noise. The bilinear focusing operator is used to decorrelate the signals [8] and to estimate the coherent signal subspace [8, 9]. From the exact solution of the acoustic scattered field [10, 11], we have derived a new source steering vector including both range and bearing of the objects. This source steering vector is employed in MUSIC algorithm instead of the classical plane wave model. The acoustic scattered field model has been addressed in many published works in several configurations, as single [12, 13] or multiple objects [14, 15], buried or partially buried objects [16, 17], with cylindrical [11, 12] or spherical shape [10, 11, 13], all those scattering models can be used with the proposed source steering vector.

The organization of this paper is as follows: the problem is formulated in Section 2. In Section 3, the scattering models are presented. In Section 4, the cumulant-based coherent signal subspace method for bearing and range estimation is presented. Experimental setup and the obtained results supporting our conclusions and demonstrating our method are provided in Sections 5 and 6. Finally, conclusion is presented in Section 7.

Throughout the paper, lowercase boldface letters represent vectors, uppercase boldface letters represent matrices, and lower- and uppercase letters represent scalars. The symbol "T" is used for transpose operation, the superscript "$+$" is used to denote complex conjugate transpose, the superscript "$*$" is used to denote complex conjugate, and $\| \cdot \|$ denotes the L_2 norm for complex vectors.

2. PROBLEM FORMULATION

We consider a linear array of N sensors (Figure 1) which receive the wideband signals scattered from P objects ($N > P$) in the presence of an additive Gaussian noise. Using vector notation, the Fourier transforms of the outputs of the array can be written as [6, 7, 18]

$$\mathbf{r}(f_n) = \mathbf{A}(f_n)\mathbf{s}(f_n) + \mathbf{b}(f_n), \quad \text{for } n = 1,\ldots,L, \quad (1)$$

where

$$
\begin{aligned}
\mathbf{A}(f_n) &= [\mathbf{a}(f_n,\theta_1,\rho_1),\mathbf{a}(f_n,\theta_2,\rho_2),\ldots,\mathbf{a}(f_n,\theta_P,\rho_P)], \\
\mathbf{s}(f_n) &= [s_1(f_n),s_2(f_n),\ldots,s_P(f_n)]^T, \\
\mathbf{b}(f_n) &= [b_1(f_n),b_2(f_n),\ldots,b_N(f_n)]^T.
\end{aligned}
\quad (2)
$$

$\mathbf{s}(f_n)$ is the vector of the source signals. $\mathbf{b}(f_n)$ is the vector of Gaussian noises which are assumed statistically independent of the source signals. $\mathbf{A}(f_n)$ is the transfer matrix which is computed from $\mathbf{a}(f_n,\theta_k,\rho_k)$ for $k = 1,\ldots,P$ given by

$$
\begin{aligned}
&\mathbf{a}(f_n,\theta_k,\rho_k) \\
&= [a(f_n,\theta_{k1},\rho_{k1}),a(f_n,\theta_{k2},\rho_{k2}),\ldots,a(f_n,\theta_{kN},\rho_{kN})]^T,
\end{aligned}
\quad (3)
$$

where θ_k and ρ_k are the bearing and the range of the kth object to the first sensor of the array, thus, $\theta_k = \theta_{k1}$ and $\rho_k = \rho_{k1}$.

A fourth-order cumulant is given by

$$
\begin{aligned}
&\text{Cum}\,(r_{k_1},r_{k_2},r_{l_1},r_{l_2}) \\
&= \text{E}\,\{r_{k_1}r_{k_2}r_{l_1}^*r_{l_2}^*\} - \text{E}\,\{r_{k_1}r_{l_1}^*\}\,\text{E}\,\{r_{k_2}r_{l_2}^*\} \\
&\quad - \text{E}\,\{r_{k_1}r_{l_2}^*\}\,\text{E}\,\{r_{k_2}r_{l_1}^*\},
\end{aligned}
\quad (4)
$$

where Cum$(\cdot)$ denotes the cumulant, r_{k_1} is the k_1 element in the vector $\mathbf{r}$, and E$\{\cdot\}$ denotes the expectation operator. The indices k_2, l_1, and l_2 are similarly defined as k_1 has been just defined. The cumulant matrix consisting of all possible permutations of the four indices $\{k_1,k_2,l_1,l_2\}$ is given in [19]
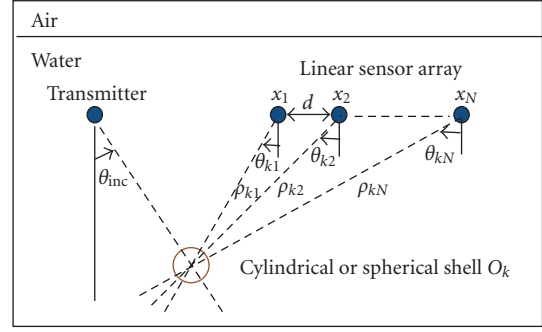

FIGURE 1: Geometry configuration of the kth object localization.

as

$$
\begin{aligned}
\mathbf{C}(f_n) &\triangleq \sum_{k=1}^{P} (\mathbf{a}(f_n,\theta_k,\rho_k) \otimes \mathbf{a}^*(f_n,\theta_k,\rho_k))u_k(f_n) \\
&\quad \times (\mathbf{a}(f_n,\theta_k,\rho_k) \otimes \mathbf{a}^*(f_n,\theta_k,\rho_k))^+,
\end{aligned}
\quad (5)
$$

where $\otimes$ is the Kronecker product and $u_k(f_n)$ is the source kurtosis (i.e., fourth-order analog of variance) of the kth complex amplitude source defined by

$$u_k(f_n) = \text{Cum}\,(s_k(f_n),s_k^*(f_n),s_k(f_n),s_k^*(f_n)). \quad (6)$$

In order to reduce the calculating time, instead of using the cumulant matrix $\mathbf{C}(f_n)$, a cumulant slice matrix ($N \times N$) of the observation vector at frequency f_n can be calculated and it offers the same algebraic properties as $\mathbf{C}(f_n)$. This matrix is denoted by $\mathbf{C}_1(f_n)$ [6, 19, 20]. We consider a cumulant slice, for example, by using the first row of $\mathbf{C}(f_n)$ and reshape it into an ($N \times N$) Hermitian matrix [20], that is,

$$
\begin{aligned}
\mathbf{C}_1(f_n) &\triangleq \text{Cum}\,(r_1(f_n),r_1^*(f_n),\mathbf{r}(f_n),\mathbf{r}^+(f_n)) \\
&= \begin{bmatrix} c_{1,1} & c_{1,N+1} & \cdots & c_{1,N^2-N+1} \\ c_{1,2} & c_{1,N+2} & \cdots & c_{1,N^2-N+2} \\ \vdots & \vdots & \vdots & \vdots \\ c_{1,N} & c_{1,2N} & \cdots & c_{1,N^2} \end{bmatrix} \\
&= \mathbf{A}(f_n)\mathbf{U}_s(f_n)\mathbf{A}^+(f_n),
\end{aligned}
\quad (7)
$$

where $c_{1,j}$ is the $(1,j)$ element of the cumulant matrix $\mathbf{C}(f_n)$ and $\mathbf{U}_s(f_n)$ is the diagonal kurtosis matrix, its ith element defined as $\text{Cum}(s_i(f_n),s_i^*(f_n),s_i(f_n),s_i^*(f_n))$ with $i = 1,\ldots,P$.

$\mathbf{C}_1(f_n)$ can be reported as the classical cross-spectral matrix [8, 21] of received data. In practice, the noise is not often white, hence the interest on the higher-order statistics is as shown in (7) in which the fourth-order cumulant matrix is not affected by additive Gaussian noise. Let $\{\lambda_i(f_n)\}_{i=1,\ldots,N}$ and $\{\mathbf{v}_i(f_n)\}_{i=1,\ldots,N}$ be the eigenvalues and the corresponding eigenvectors of the matrix $\mathbf{C}_1(f_n)$, respectively, then the eigendecomposition of $\mathbf{C}_1(f_n)$ can be expressed as

$$\mathbf{C}_1(f_n) = \sum_{i=1}^{N} \lambda_i(f_n)\mathbf{v}_i(f_n)\mathbf{v}_i^+(f_n). \quad (8)$$

In matrix representation, (8) can be written

$$\mathbf{C}_1(f_n) = \mathbf{V}(f_n)\mathbf{\Lambda}(f_n)\mathbf{V}^+(f_n), \qquad (9)$$

where

$$\begin{aligned} \mathbf{V}(f_n) &= [\mathbf{v}_1(f_n),\ldots,\mathbf{v}_N(f_n)], \\ \mathbf{\Lambda}(f_n) &= \mathrm{diag}(\lambda_1(f_n),\ldots,\lambda_N(f_n)). \end{aligned} \qquad (10)$$

Assuming that the columns of $\mathbf{A}(f_n)$ are linearly independent, in other words, $\mathbf{A}(f_n)$ is full rank, it follows that for nonsingular $\mathbf{C}_1(f_n)$, the rank of $\mathbf{A}(f_n)\mathbf{U}_s(f_n)\mathbf{A}^+(f_n)$ is P. This rank property implies that:

(i) the $(N - P)$ multiplicity of its smallest eigenvalues

$$\lambda_{P+1}(f_n) = \cdots = \lambda_N(f_n) \cong 0; \qquad (11)$$

(ii) the eigenvectors corresponding to the minimal eigenvalues are orthogonal to the columns of the matrix $\mathbf{A}(f_n)$,

$$\begin{aligned} \mathbf{V}_b(f_n) &\triangleq \{\mathbf{v}_{P+1}(f_n),\ldots,\mathbf{v}_N(f_n)\} \\ &\perp \{\mathbf{a}(f_n,\theta_1,\rho_1),\ldots,\mathbf{a}(f_n,\theta_P,\rho_P)\}. \end{aligned} \qquad (12)$$

The MUSIC method [18] is based on the above property and it has been widely used to estimate the directions of the arrival of the sources. The spatial spectrum of the MUSIC method [18], in the case of narrowband signals ($L = 1$), is given by

$$\mathrm{MUSIC}\,(f_1,\theta_k) = \frac{1}{\|\mathbf{g}^+(f_1,\theta_k)\mathbf{V}_b(f_1)\|^2}, \qquad (13)$$

where $\mathbf{g}$ is the steering vector which can be filled with plane wave model when the sources are in the far-field zone of the sensor array [18].

In this study, we have extended firstly the MUSIC method [18] to estimate simultaneously range and bearing of the objects using narrowband signals by including the acoustic scattering model of the objects. We have called this modified algorithm the MUSIC NB method and in the same manner its spatial spectrum is given by

$$\mathrm{MUSIC\,NB}(f_1,\theta_k,\rho_k) = \frac{1}{\|\mathbf{a}^+(f_1,\theta_k,\rho_k)\mathbf{V}_b(f_1)\|^2}. \qquad (14)$$

Then, in the following sections, we will present how to fill the vector of the scattering model $\mathbf{a}(f_1,\theta_k,\rho_k)$ and how to use the focusing slice cumulant matrix (wideband signals) to improve the object localization.

3. SCATTERING MODEL

Consider the case in which a plane wave is incident, with an angle θ_{inc}, on P infinite elastic cylindrical shells or elastic spherical shells of inner radius β_k and outer radius α_k for $k = 1,\ldots,P$, located in a free space at (θ_k,ρ_k) the bearing and the range of the kth object, associated with the first sensor

of the array x_1 (Figure 1). The fluid outside the shells is labeled by 1, thus, the sound velocity is denoted by c_1 and the wavenumber is $K_{n1} = 2\pi f_n/c_1$.

3.1. Cylindrical shell

We consider the case of infinitely long cylindrical shell. In order to calculate the exact solution for the acoustic scattered field $a_{\mathrm{cyl}}(f_n,\theta_{k1},\rho_{k1})$, a partial wave series decomposition is used. The scattered pressure, in the case of normal incidence, is given by [11, 12]

$$\begin{aligned} &a_{\mathrm{cyl}}(f_n,\theta_{k1},\rho_{k1}) \\ &= p_{c0}\sum_{m=0}^{\infty} j^m H_m^{(1)}(K_{n1}\rho_{k1})\epsilon_m b_m \cos\,(m(\theta_{k1} - \theta_{\mathrm{inc}})), \end{aligned} \qquad (15)$$

where p_{c0} is a constant, $\epsilon_0 = 1$, $\epsilon_1 = \epsilon_2 = \cdots = 2$, b_m is a coefficient depending on boundary conditions, $H_m^{(1)}$ is the cylindrical first kind Hankel function, and m is the modal order [12].

The scattering model in (15) is very inaccurate for modeling finite cylinders because of end-cap effects [22–24] and also for oblique incidence [25].

3.2. Spherical shell

The analysis is now extended to the case where the scatterer is a spherical shell. The scattered pressure is given by [10, 11, 13]

$$\begin{aligned} &a_{\mathrm{sph}}(f_n,\theta_{k1},\rho_{k1}) \\ &= p_{s0}\sum_{m=0}^{\infty} j^m(2m+1)h_m^{(1)}(K_{n1}\rho_{k1})B_m P_m(\cos(\theta_{k1} - \theta_{\mathrm{inc}})), \end{aligned} \qquad (16)$$

where p_{s0} is a constant, $h_m^{(1)}$ is the spherical first kind Hankel function, and $P_m(\cos(\theta_{k1} - \theta_{\mathrm{inc}}))$ is the Legendre polynomial [13].

The vector $\mathbf{a}(f_n,\theta_k,\rho_k)$ filled with the cylindrical scattering model in the case of cylindrical shells and filled with the spherical scattering model in the case of spherical shells. For example, when the considered objects are cylindrical shells, this vector is given by

$$\mathbf{a}(f_n,\theta_k,\rho_k) = [a_{\mathrm{cyl}}(f_n,\theta_{k1},\rho_{k1}),\ldots,a_{\mathrm{cyl}}(f_n,\theta_{kN},\rho_{kN})]^T. \qquad (17)$$

Equations (15) and (16) give the first component of the vector $\mathbf{a}(f_n,\theta_k,\rho_k)$. Thus, in a similar manner, the other components $a_{\mathrm{cyl}}(f_n,\theta_{ki},\rho_{ki})$ and $a_{\mathrm{sph}}(f_n,\theta_{ki},\rho_{ki})$ for $i = 2,\ldots,N$, associated with the ith sensor, can be formed, where all the couples (θ_{ki},ρ_{ki}) are calculated using the general Pythagorean theorem and are functions of the couple (θ_{k1},ρ_{k1}). Thus, the used configuration is shown in Figure 1. The obtained θ_{ki},ρ_{ki}

are given by

$$\rho_{ki} = \sqrt{\rho_{ki-1}^2 - d^2 - 2\rho_{ki-1}d\cos\left(\frac{\pi}{2} + \theta_{ki-1}\right)},$$
$$\theta_{ki} = \cos^{-1}\left[\frac{d^2 + \rho_{ki}^2 - \rho_{ki-1}^2}{2\rho_{ki-1}d}\right], \tag{18}$$

where d is the distance between two adjacent sensors.

Equation (18) is employed in (14) to estimate simultaneously range and bearing of the objects using narrowband signals. In the following section, we will present how to include the focusing slice cumulant matrix to treat correlated wideband signals.

4. CUMULANT-BASED COHERENT SIGNAL SUBSPACE METHOD FOR BEARING AND RANGE ESTIMATION

In this section, the frequency diversity of wideband signals is considered. The received signals come from the reflections on the objects, thus, these signals are totally correlated and the MUSIC method looses its performances if any preprocessing is used before as the spatial smoothing [21] or the frequential smoothing [8, 26]. It appears clearly that it is necessary to apply any preprocessing to decorrelate the signals. According to the published results [21], the spatial smoothing needs a greater number of sensors than the frequential smoothing. In this section, the employed signals are wideband. This choice is made in order to decorrelate the signals by means of an average of the focused slice cumulant matrices. Therefore, the objects can be localized even if the received signals are totally correlated. This would have not been possible with the narrowband signals without the spatial smoothing. In the frequential smoothing-based processing framework [18, 21, 27], we have adopted the optimal method which is the bilinear focusing operator [8, 26], in order to obtain the coherent signal subspace. This technique divides the frequency band into L narrowbands [8, 26], then transforms the received signals in the L bands into the focusing frequency f_0. The average of the focused signals is then calculated and consequently decorrelates the signals [9, 28]. Here, f_0 is the midband frequency of the spectrum of the received signal and it is chosen as the focusing frequency.

The number P of the sources is estimated using the well-known AIC or MDL criterion [29]. The following is the step-by-step description of the proposed method which we have called the MUSIC WB method:

(1) use the beamformer method to find an initial estimate of θ_k, where $k = 1, \ldots, K$, with $K \leq P$,
(2) compute the initial values of $\rho_k = X/\cos(\theta_k)$ for $k = 1, \ldots, K$, where X represents the distance between the receiver and the bottom of the tank,
(3) fill the transfer matrix

$$\hat{\mathbf{A}}(f_n) = [\mathbf{a}(f_n, \theta_1, \rho_1), \mathbf{a}(f_n, \theta_2, \rho_2), \ldots, \mathbf{a}(f_n, \theta_K, \rho_K)], \tag{19}$$

where each component of the directional vector $\mathbf{a}(f_n, \theta_k, \rho_k)$ for $k = 1, \ldots, K$ is filled using (15) or (16) considering the object shape,

(4) estimate the cumulant slice matrix of the received data $\mathbf{C}_1(f_n)$ using (7) and perform its eigendecomposition,
(5) calculate diagonal kurtosis matrix at each frequency f_n by using (7) and obtain

$$\mathbf{U}_s(f_n)$$
$$= (\hat{\mathbf{A}}^+(f_n)\hat{\mathbf{A}}(f_n))^{-1}\hat{\mathbf{A}}^+(f_n)[\mathbf{C}_1(f_n)]\hat{\mathbf{A}}(f_n)(\hat{\mathbf{A}}^+(f_n)\hat{\mathbf{A}}(f_n))^{-1},$$

$$\tag{20}$$

(6) calculate the average of the diagonal kurtosis matrices

$$\overline{\mathbf{U}}_s(f_0) = \frac{1}{L}\sum_{n=1}^{L}\mathbf{U}_s(f_n), \tag{21}$$

(7) calculate $\hat{\mathbf{C}}_1(f_0) = \hat{\mathbf{A}}(f_0)\overline{\mathbf{U}}_s(f_0)\hat{\mathbf{A}}^+(f_0)$,
(8) form the focusing operator using the eigenvectors

$$\mathbf{T}(f_0, f_n) = \hat{\mathbf{V}}(f_0)\mathbf{V}^+(f_n), \tag{22}$$

where $\mathbf{V}(f_n)$ and $\hat{\mathbf{V}}(f_0)$ are the eigenvectors of the cumulant matrices $\mathbf{C}_1(f_n)$ and $\hat{\mathbf{C}}_1(f_0)$, respectively,

(9) form the average slice cumulant matrix $\overline{\mathbf{C}}_1(f_0)$ and perform its eigendecomposition

$$\overline{\mathbf{C}}_1(f_0) = \frac{1}{L}\sum_{n=1}^{L}\mathbf{T}(f_0, f_n)\mathbf{C}_1(f_n)\mathbf{T}^+(f_0, f_n), \tag{23}$$

(10) estimate the number P of objects using AIC or MDL criterion with the eigenvalues of matrix $\overline{\mathbf{C}}_1(f_0)$,
(11) calculate the spatial spectrum of the MUSIC WB method for estimating range and bearing of the objects using

$$\text{MUSIC WB}(f_0, \theta_k, \rho_k) = \frac{1}{\|\mathbf{a}(f_0, \theta_k, \rho_k)^+\overline{\mathbf{V}}_b(f_0)\|^2}, \tag{24}$$

where $\overline{\mathbf{V}}_b(f_0)$ is the eigenvector matrix of $\overline{\mathbf{C}}_1(f_0)$ associated with the $(N - P)$ smallest eigenvalues.

5. EXPERIMENTAL SETUP

The data has been recorded using an experimental water tank (Figure 2) in order to evaluate the performances of the developed method.

The transmitter sensor (on the left in Figure 2) is fixed at an incident angle $\theta_{\text{inc}} = 60°$ and has a beamwidth equal to 5°. The receiver sensor (on the right in Figure 2) is omnidirectional and moves horizontally along the XX' axis, step by step, from the initial to the final position (Figure 3) with a step size $d = 0.002$ m and takes ten positions in order to form a uniform linear array of sensors with $N = 10$. The transmitted signal has the following properties: impulse duration is 15 us, the frequency band is $B_f = [f_{\min} = 150, f_{\max} = 250]$ kHz and the sampling rate is 2 MHz. The duration of the received signals is 700 us. This tank is filled with water with $W_h = 0.5$ m (Figure 2) and its bottom is filled with homogeneous fine sand, where three cylinder couples
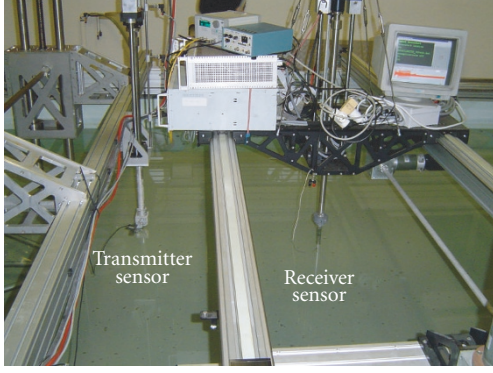
FIGURE 2: Experimental tank.

FIGURE 3: Experimental setup.

$((O_3, O_4), (O_5, O_6), (O_7, O_8))$ and one sphere couple (O_1, O_2) (Figure 4) are buried. Table 1 summarizes the characteristics of these objects. The acoustic wave velocity in the water tank is $c_1 = 1466$ m/s.

The experiment configuration in the scaled tank is realistic. In order to reproduce the configuration at a real scenario (rs), we should take $W_{h(\mathrm{rs})}/\delta_{0(\mathrm{rs})} = W_h/\delta_0$, where $\delta_0 = c_1/f_0$, and $W_{h(\mathrm{rs})}$ is the water depth, and $\delta_{0(\mathrm{rs})}$ is the wavelength in a real scenario. For that the distance d between two consecutive sensors, the object dimensions, and the burial depth used in the experimental tank must be multiplied by $\delta_{0(\mathrm{rs})}/\delta_0$.

The cylinders used satisfy the approximation such that they can be considered infinitely long. Indeed, their lengths satisfy the following condition [30]:

$$l_{O_k} > 2\sqrt{\rho_{\max}\delta_{\max}}, \tag{25}$$

where $\delta_{\max} \simeq 0.01$ m is the maximal wavelength and $\rho_{\max}$ is the maximal range of all the objects

$$\rho_{\max} = \sqrt{(H_b + d_{\mathrm{depth}} + \alpha_{\max})^2 + (\mathrm{TR})^2}, \tag{26}$$

where $H_b = 0.4$ m is the vertical distance between the receiver and the bottom of the tank, $d_{\mathrm{depth}} = 0.005$ m is the burial depth of the objects, $\alpha_{\max} = 0.02$ m is the outer radius of the biggest object (object O_7 or O_8), and $\mathrm{TR} = 0.9$ m is the horizontal distance between the transmitter and the final position of the receiver (Figure 3), thus, $\rho_{\max} = 0.99$ m and $l_{O_k} > 0.19$ m for all $k = 1, \ldots, 8$.

The homogeneous fine sand used in this study has geoacoustic characteristics near to those of water. Consequently, we can make the assumption that the objects are in a free space. However, this assumption remains valid only when the presence of the water/sediment interface has negligible effects on the results. Otherwise, acoustic scattering model including the water/sediment interface effects [31–34] must be used. The considered objects are made of dural aluminum with density $D_2 = 1800$ kg/m^3, the longitudinal and transverse elastic-wave velocities inside the shell medium are $c_l = 6300$ m/s and $c_t = 3200$ m/s, respectively. The external fluid is water with density $D_1 = 1000$ kg/m^3 and the internal
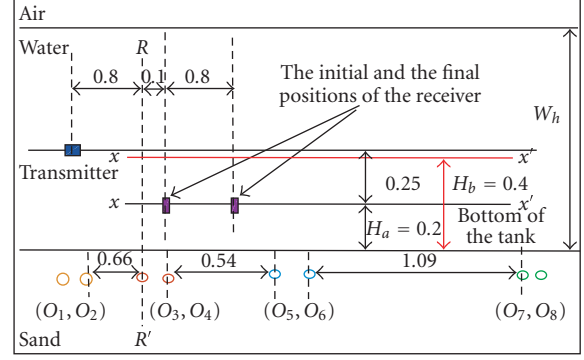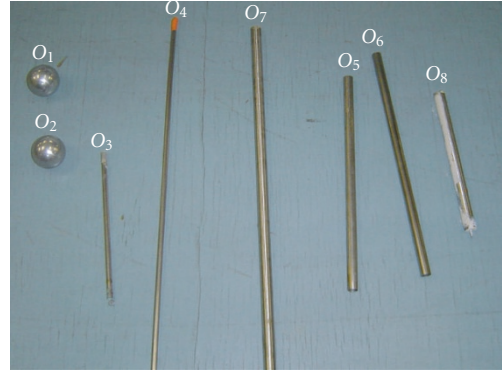

FIGURE 4: Objects.

fluid is water or air with density $D_{3\mathrm{air}} = 1.2\ 10^{-6}$ kg/m^3 or $D_{3\mathrm{water}} = 1000$ kg/m^3.

The experimental setup is shown in Figure 3, where all the dimensions are given in meter. First, we have buried the considered objects in the sand at 0.005 m. Then, we have done eight experiments that we have called $E_{i(O_{ii}, O_{ii+1})}$, where $i = 1, \ldots, 8$ and $ii = 1, 3, 5, 7$. Two experiments are performed for each couple: one, when the receiver horizontal axis XX' is fixed at 0.2 m from the bottom of the tank $(E_{1(O_1, O_2)}, \ldots, E_{4(O_7, O_8)})$, the other when this axis is fixed at 0.4 m from the bottom of the tank $(E_{5(O_1, O_2)}, \ldots, E_{6(O_7, O_8)})$. RR' is a vertical axis which goes through the center of the first object of each couple. Note that the configuration shown in Figure 3 is associated with the experiment $E_{2(O_3, O_4)}$, where RR' axis goes through the object O_3. Thus, for each experiment, only one object couple is radiated by the transmitter sensor. At each sensor, time-domain data corresponding only to target echoes are collected with signal-to-noise ratio equal to 20 dB. The typical sensor output signals recorded during one experiment are shown in Figure 5. Figure 6 shows an example of the power spectral density of the received signal on fifth sensor.

TABLE 1: Characteristics of the various objects (the inner radius $\beta_{O_k} = \alpha_{O_k} - 0.001$ m, for $k = 1, \ldots, 8$).

	First couple Spheres (O_1, O_2)	Second couple Cylinders (O_3, O_4)
Outer radius (m)	$\alpha_{O_{1,2}} = 0.03$	$\alpha_{O_{3,4}} = 0.01$
Length (m)	—	$l_{O_3} = 0.258$ $l_{O_4} = 0.69$
Filled with	Air	Air
Separated by (m)	0.33	0.13
	Third couple Cylinders (O_5, O_6)	Fourth couple Cylinders (O_7, O_8)
Outer radius (m)	$\alpha_{O_{5,6}} = 0.018$	$\alpha_{O_{7,8}} = 0.02$
Length (m)	$l_{O_5} = 0.372$ $l_{O_6} = 0.396$	$l_{O_7} = 0.63$ $l_{O_8} = 0.24$
Filled with	Water	Air
Separated by (m)	0.16	0.06

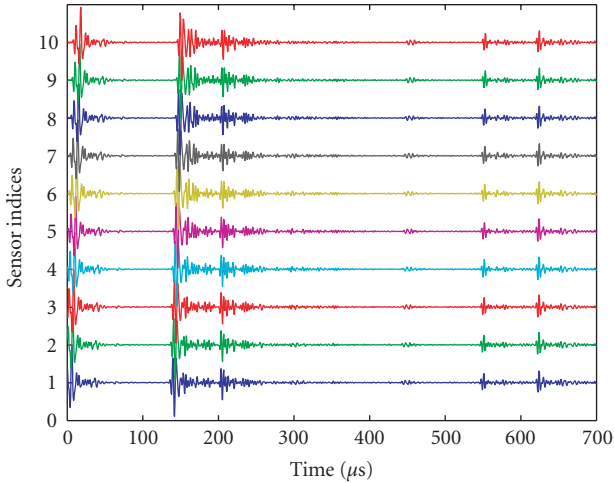FIGURE 6: Power spectral density of the signal received on fifth sensor.

FIGURE 5: Observed sensor output signals.

6. RESULTS AND DISCUSSION

The steps listed above in Section 4 were applied on each experimental data set, thus, an initialization of θ, using the beamformer, and of ρ, using $X/\cos(\theta)$, has been done, where X is the distance between the receiver axis XX' and the bottom of the tank. The distance X can take two values H_a or H_b. For example, for the experiment $E_{1(O_1, O_2)}$, those two parameters have been initialized by $\theta_1 = 15°$, $\rho_1 = 0.28$ m, and $X = H_a = 0.2$ m. Moreover, the average of the focused slice cumulant matrices was calculated using $L = 50$ frequencies chosen in the frequency band of interest $[f_{\min}, f_{\max}]$. The data length to estimate the cumulant matrix is 1400 samples. Thanks to the detection AIC criterion [29], two sources are detected ($P = 2$). Then, a sweeping is made on the bearing from $-90°$ to $90°$ with a step of $0.1°$, as well as on the range from 0.2 to 1.5 m with a step of 0.002 m. Two examples of
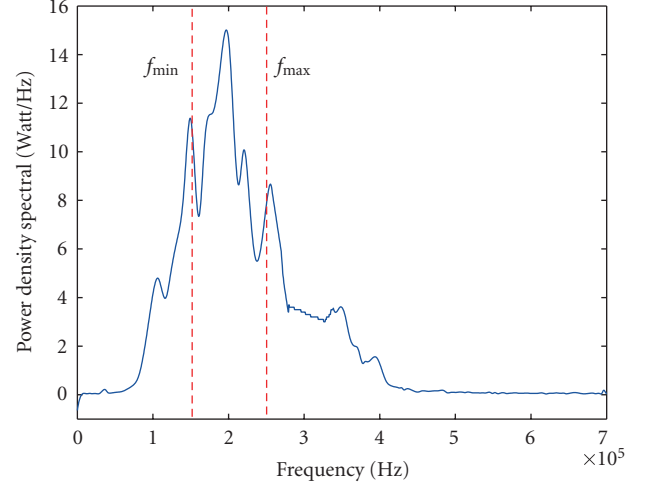
the obtained spatial spectra using the MUSIC WB method are shown in Figures 7(a)-7(b).

Table 2 summarizes the expected and the estimated range and bearing of the objects obtained using the MUSIC method ((13) with $f_1 = 200$ kHz), the MUSIC NB method ((14) with $f_1 = 200$ kHz), and the MUSIC WB method (24). The indices 1 and 2 are the first and the second objects of each couple of cylinders or spheres. The presented values are the spatial spectrum peaks coordinate on the bearing-range plane. Note that the bearing objects obtained after applying the MUSIC method are not exploitable. Similar results were obtained when we applied the MUSIC NB method because the received signals are correlated. However, satisfying results were obtained when we applied the MUSIC WB method, thus, bearing and range of the objects were successfully estimated. In order to a posteriori verify the quality of estimation of the MUSIC WB method, it is possible to use the relative error (RE) defined as follows:

$$\text{RE}_{\text{WB}y_i} = \frac{|y_{i\exp} - y_{i\text{est}}|}{|y_{i\exp}|} \quad \text{for } i = 1, 2, \quad (27)$$

where $y_{i\exp}$ (resp., $y_{i\text{est}}$) represents the ith expected (resp., the ith estimated) value of θ or ρ. The obtained values of RE for θ and ρ are given in Table 2. These values confirm the efficiency of the proposed method.

7. CONCLUSION

In this paper, we proposed a new method to estimate both bearing and range of the sources in a noisy environment and in presence of correlated signals. To cope with the noise problem, we have used higher-order statistics, thus, we have formed the slice cumulant matrices at each frequency bin. Then, we have applied the coherent subspace method which consists in a frequential smoothing in order to cope with the signal correlation problem and in forming the focusing slice cumulant matrix. To estimate range and bearing,
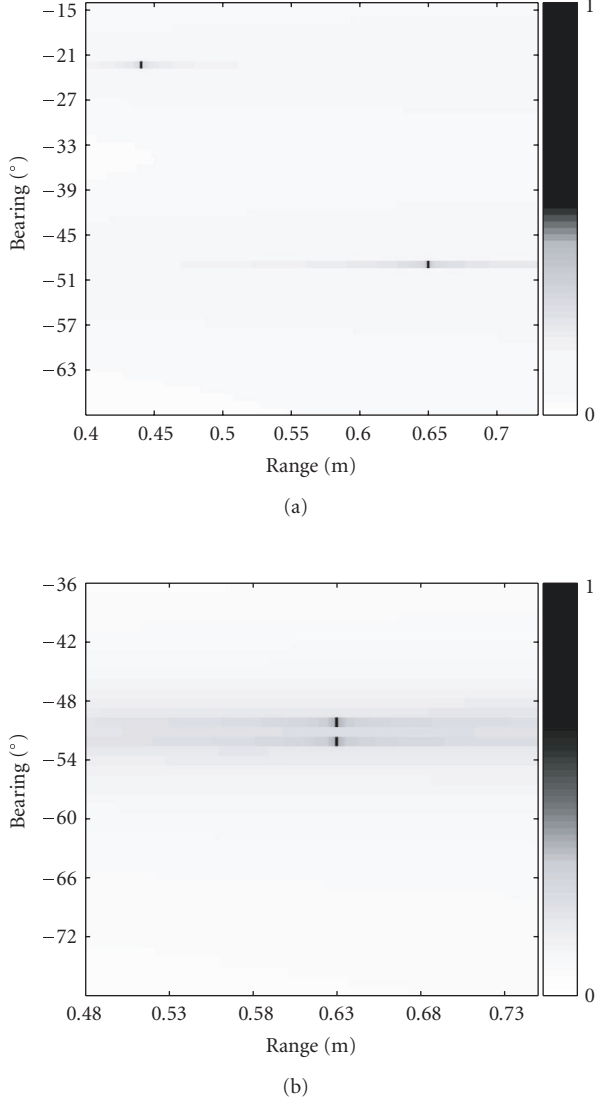
(a)

(b)

FIGURE 7: Spatial spectra of the developed method: zoom in range-bearing plane. (a) $E_{5(O_1,O_2)}$, (b) $E_{8(O_7,O_8)}$.

TABLE 2: The expected (exp) and estimated (est) values of range and bearing objects (negative bearing is clockwise from the vertical).

	$E_{1(O_1,O_2)}$	$E_{2(O_3,O_4)}$	$E_{3(O_5,O_6)}$	$E_{4(O_7,O_8)}$
$\theta_{1\,exp}(°)$	−26.5	−23	−33.2	−32.4
$\rho_{1\,exp}(m)$	0.24	0.24	0.26	0.26
$\theta_{2\,exp}(°)$	44	9.2	−20	5.8
$\rho_{2\,exp}(m)$	0.31	0.22	0.24	0.22
MUSIC				
$\theta_{1\,est}(°)$	−18	−30	−40	−22
$\theta_{2\,est}(°)$	30	−38	−48	−32
MUSIC NB				
$\theta_{1,2\,est}(°)$	15	−12	−28	−10
$\rho_{1,2\,est}(m)$	0.28	0.23	0.25	0.24
MUSIC WB				
$\theta_{1\,est}(°)$	−26	−23	−33	−32
$\rho_{1\,est}(m)$	0.22	0.25	0.29	0.28
$\theta_{2\,est}(°)$	43	9	−20	6
$\rho_{2\,est}(m)$	0.34	0.25	0.25	0.23
$RE_{WB\,\theta_1}$	0.018	0	0.006	0.012
$RE_{WB\,\rho_1}$	0.083	0.041	0.11	0.076
$RE_{WB\,\theta_2}$	0.022	0.021	0	0.034
$RE_{WB\,\rho_2}$	0.096	0.13	0.041	0.045
	$E_{5(O_1,O_2)}$	$E_{6(O_3,O_4)}$	$E_{7(O_5,O_6)}$	$E_{8(O_7,O_8)}$
$\theta_{1\,exp}(°)$	−50	−52.1	−70	−51.6
$\rho_{1\,exp}(m)$	0.65	0.65	1.24	0.65
$\theta_{2\,exp}(°)$	−22	−41	−65.3	−49
$\rho_{2\,exp}(m)$	0.45	0.56	1.17	0.64
MUSIC				
$\theta_{1\,est}(°)$	−58	25	−40	−45
$\theta_{2\,est}(°)$	−12	−40	−45	−45
MUSIC NB				
$\theta_{1,2\,est}(°)$	−35	−45	−70	−50
$\rho_{1,2\,est}(m)$	0.52	0.63	1.2	0.65
MUSIC WB				
$\theta_{1\,est}(°)$	−49	−52	−70	−52
$\rho_{1\,est}(m)$	0.65	0.63	1.21	0.63
$\theta_{2\,est}(°)$	−22	−40	−65	−50
$\rho_{2\,est}(m)$	0.44	0.53	1.2	0.63
$RE_{WB\,\theta_1}$	0.02	0.019	0	0.007
$RE_{WB\,\rho_1}$	0	0.03	0.024	0.03
$RE_{WB\,\theta_2}$	0	0.024	0.004	0.002
$RE_{WB\,\rho_2}$	0.022	0.053	0.025	0.015

the focusing slice cumulant matrix was used instead of using the spectral matrix and the exact solution of the acoustic scattered field was used instead of the plane wave model, in the MUSIC method. The performances of this method were investigated through scaled tank tests associated with many spherical and cylindrical shells buried in an homogenous fine sand. The obtained results show that the proposed method is superior in terms of bearing and range estimation compared with the classical MUSIC algorithm. Range and bearing of the objects were estimated with a significantly good accuracy thanks to the free space assumption. Opening directions for future work could concern mainly the performances of the proposed method under some more realistic experimental conditions. We could improve the scattering model by including the water/sediment interface effects and considering the influence of the signal-to-reverberation ratio. In order to facilitate the implementation of the proposed method in real-time application, the reduction of computational time should be considered in the future study. For example, the high-resolution methods without eigendecomposition could be used.

REFERENCES

[1] G. Nicq and M. Brussieux, "A time-frequency method for classifying objects at low frequencies," in *Proceedings of the IEEE Oceans Conference*, vol. 1, pp. 148–152, Nice, France, September-October 1998.

[2] R. Guillermin, P. Lasaygues, J. Sessarego, and A. Wirgin, "Characterization of buried objects by a discretized domain integral equation inversion method using born approximation," in *Proceedings of the 5th European Conference on Underwater Acoustics (ECUA '00)*, vol. 2, pp. 863–868, Lyon, France, July 2000.

[3] A. Hetet, M. Amate, B. Zerr, et al., "SAS processing results for the detection of buried objects with a ship-mounted sonar," in *Proceedings of the 7th European Conference on Underwater Acoustics (ECUA '04)*, pp. 1127–1132, Delft, The Netherlands, July 2004.

[4] P. Roux and M. Fink, "Time reversal in a waveguide: study of the temporal and spatial focusing," *The Journal of the Acoustical Society of America*, vol. 107, no. 5, pp. 2418–2429, 2000.

[5] A. Derode, A. Tourin, and M. Fink, "Limits of time-reversal focusing through multiple scattering: long-range correlation," *The Journal of the Acoustical Society of America*, vol. 107, no. 6, pp. 2987–2998, 2000.

[6] E. Gonen and J. M. Mendel, "Applications of cumulants to array processing—Part III: blind beamforming for coherent signals," *IEEE Transactions on Signal Processing*, vol. 45, no. 9, pp. 2252–2264, 1997.

[7] J. M. Mendel, "Tutorial on higher-order statistics (spectra) in signal processing and system theory: theoretical results and some applications," *Proceedings of the IEEE*, vol. 79, no. 3, pp. 278–305, 1991.

[8] S. Valaee and P. Kabal, "Wideband array processing using a two-sided correlation transformation," *IEEE Transactions on Signal Processing*, vol. 43, no. 1, pp. 160–172, 1995.

[9] H. Wang and M. Kaveh, "Coherent signal-subspace processing for the detection and estimation of angles of arrival of multiple wide-band sources," *IEEE Transactions on Acoustics, Speech, and Signal Processing*, vol. 33, no. 4, pp. 823–831, 1985.

[10] J. A. Fawcett, W. L. J. Fox, and A. Maguer, "Modeling of scattering by objects on the seabed," *The Journal of the Acoustical Society of America*, vol. 104, no. 6, pp. 3296–3304, 1998.

[11] M. C. Junger, "Sound scattering by thin elastic shells," *The Journal of the Acoustical Society of America*, vol. 24, no. 4, pp. 366–373, 1952.

[12] R. D. Doolittle and H. Überall, "Sound scattering by elastic cylindrical shells," *The Journal of the Acoustical Society of America*, vol. 39, no. 2, pp. 272–275, 1966.

[13] R. Goodman and R. Stern, "Reflection and transmission of sound by elastic spherical shells," *The Journal of the Acoustical Society of America*, vol. 34, no. 3, pp. 338–344, 1962.

[14] C. Prada and M. Fink, "Separation of interfering acoustic scattered signals using the invariants of the time-reversal operator. Application to Lamb waves characterization," *The Journal of the Acoustical Society of America*, vol. 104, no. 2, pp. 801–807, 1998.

[15] Z. Ye, "Recent developments in underwater Acoustics: acoustic scattering from single and multiple bodies," *Proceedings of the National Science Council, Republic of China, Part A: Physical Science and Engineering*, vol. 25, no. 3, pp. 137–150, 2001.

[16] R. Lim, J. L. Lopes, R. H. Hackman, and D. G. Todoroff, "Scattering by objects buried in underwater sediments: theory and experiment," *The Journal of the Acoustical Society of America*, vol. 93, no. 4, pp. 1762–1783, 1993.

[17] A. Tesei, A. Maguer, W. L. J. Fox, R. Lim, and H. Schmidt, "Measurements and modeling of acoustic scattering from partially and completely buried spherical shells," *The Journal of the Acoustical Society of America*, vol. 112, no. 5, pp. 1817–1830, 2002.

[18] A. Bendjama, S. Bourennane, and M. Frikel, "Direction finding after blind identification of source steering vectors," in *Proceedings of the IASTED International Conference on Signal and Image Processing (SIP '98)*, pp. 491–494, Las Vegas, Nev, USA, October 1998.

[19] N. Yuen and B. Friedlander, "DOA estimation in multipath: an approach using fourth-order cumulants," *IEEE Transactions on Signal Processing*, vol. 45, no. 5, pp. 1253–1263, 1997.

[20] S. Bourennane, M. Frikel, and A. Bendjama, "Fast wideband source separation based on higher-order statistics," in *Proceedings of the IEEE Signal Processing Workshop on Higher Order Statistics (HOS '97)*, pp. 354–358, Banff, Canada, July 1997.

[21] S. U. Pillai and B. U. H. Kwon, "Forward/backward spatial smoothing techniques for coherent signal identification," *IEEE Transactions on Acoustics, Speech, and Signal Processing*, vol. 37, no. 1, pp. 8–15, 1989.

[22] G. Maze, D. Decultot, F. Lecroq, J. Ripoche, X.-L. Bao, and H. Uberall, "Resonance identifications of a solid axisymmetric finite length target," *The Journal of the Acoustical Society of America*, vol. 96, no. 2, pp. 944–950, 1994.

[23] M. L. Rumerman, "Contribution of membrane wave reradiation to scattering from finite cylindrical steel shells in water," *The Journal of the Acoustical Society of America*, vol. 93, no. 1, pp. 55–65, 1993.

[24] N. K. Veksler, *Resonance Acoustic Spectroscopy*, Springer, New York, NY, USA, 1993.

[25] X.-L. Bao, "Echoes and helical surface waves on a finite elastic cylinder excited by sound pulses in water," *The Journal of the Acoustical Society of America*, vol. 94, no. 3, pp. 1461–1466, 1993.

[26] M. Frikel and S. Bourennane, "Fast algorithm for the wideband array processing using twosided correlation transformation," in *Proceedings of the 8th European Signal Processing Conference (EUSIPCO '96)*, vol. 2, pp. 959–962, Trieste, Italy, September 1996.

[27] K. M. Reddy and V. U. Reddy, "Further results in spatial smoothing," *Signal Processing*, vol. 48, no. 3, pp. 217–224, 1996.

[28] H. Hung and M. Kaveh, "Focussing matrices for coherent signal-subspace processing," *IEEE Transactions on Acoustics, Speech, and Signal Processing*, vol. 36, no. 8, pp. 1272–1281, 1988.

[29] M. Wax and T. Kailath, "Detection of signals by information theoretic criteria," *IEEE Transactions on Acoustics, Speech, and Signal Processing*, vol. 33, no. 2, pp. 387–392, 1985.

[30] T. K. Stanton, "Sound scattering by cylinders of finite length. II. Elastic cylinders," *The Journal of the Acoustical Society of America*, vol. 83, no. 1, pp. 64–67, 1988.

[31] J. A. Fawcett, "Scattering from a partially fluid-filled, elastic-shelled sphere," *The Journal of the Acoustical Society of America*, vol. 109, no. 2, pp. 508–513, 2001.

[32] J. A. Fawcett and R. Lim, "Evaluation of the integrals of target/seabed scattering using the method of complex images," *The Journal of the Acoustical Society of America*, vol. 114, no. 3, pp. 1406–1415, 2003.

[33] R. Lim, K. L. Williams, and E. I. Thorsos, "Acoustic scattering by a three-dimensional elastic object near a rough surface," *The Journal of the Acoustical Society of America*, vol. 107, no. 3, pp. 1246–1262, 2000.

[34] R. Lim, "Acoustic scattering by a partially buried three-dimensional elastic obstacle," *The Journal of the Acoustical Society of America*, vol. 104, no. 2, pp. 769–782, 1998.

Zineb Saidi received the Bachelor degree's in electrical engineering in 2000 from M. Mammeri University, Tizi-Ouzou, Algeria and the Master's degree in electrical engineering in 2002 from Ecole Polythechnique de l'Université de Nantes, France. In 2002, she joined the French Naval Academy Research Institute (IRE-Nav), Brest, France as a Teaching and Research Assistant. Since 2003, she has been preparing her Ph.D. degree related to buried object localization in sediment using noninvasive techniques. Her research interests are applications of array processing and buried objects localization, namely, in underwater acoustics. She has presented several papers in this subject area at specialized international meetings.

Salah Bourennane received his Ph.D. degree from Institut National Polytechnique de Grenoble, France, in 1990, in signal processing. Currently, he is a Full Professor at the Ecole Généraliste d'Ingénieurs de Marseille, France. His research interests are in statistical signal processing, array processing, image processing, multidimensional signal processing, and performances analysis.